Supplementary Information for

# Resolving Atomic-Scale Structure and Chemical Coordination in High Entropy Alloy Electrocatalysts for Structure-Function Relationship Elucidation

Bijil Subhash[1], Raymond R. Unocic[2], Leighanne C. Gallington[3], Joshua Wright[4], Soshan Cheong[5], Richard D. Tilley[5,6] & Nicholas M. Bedford[1]*

[1]School of Chemical Engineering, University of New South Wales, Sydney, NSW 2052, Australia

[2]Center for Nanophase Materials Sciences, Oak Ridge National Laboratory, Oak Ridge, 37831, Tennessee, USA

[3]X-ray Science Division, Advanced Photon Source, Argonne National Laboratory, Argonne, Illinois 60439, United States

[4]Department of Physics, Illinois Institute of Technology, Chicago, Illinois 60616, United States

[5]Mark Wainwright Analytical Centre, University of New South Wales, Sydney, NSW 2052, Australia

[6]School of Chemistry, University of New South Wales, Sydney, NSW, 2052 Australia

*Corresponding author: n.bedford@unsw.edu.au

This supporting information contains:

- Supplementary Methods
- Supplementary Notes
- Supplementary Figures 1-18
- Supplementary Tables 1-5
- Supplementary References

# Supplementary Methods

## Calculation of bulk surface configurational entropy

Configurational entropy ($\Delta S_{conf}$) change per mole for the formation of HEAs from $n$ elements with $X_i$ mole fraction is[1]:

$$\Delta S_{conf} = -R \sum_{i=1}^{n} X_i ln X_i$$

In which R is the gas constant. The bulk composition of HEAs was calculated from ICP-MS.

## Correlation Analysis

Correlation of peptide sequences and catalytic activity with structural parameters were undertaken using the corrplot package for R. Peptide sequences were encoded as 0 and 1 for BP7A and Co2-P2, respectively.

# Supplementary Notes

## Supplementary Note 1

To verify the reliability of reverse Monte Carlo generated structure models, bulk Au-M (M-Pt/Pd/Au/Co/Sn/Ce) coordination number ($N_{Au-M}$) obtained from RMC simulation of HEAs were used as the fitting constraints to extended X-ray absorption fine structure spectroscopy (EXAFS) curve fitting (**Supplementary Fig. 7-8)**. EXAFS curve fitting has resulted in the evaluation of free EXAFS parameters; Debye Waller factor ($\sigma$), energy shift ($\Delta E$) and interatomic shift in distance from theoretical model ($\Delta R_{Au-M}$) (**Supplementary Table 2)**. The quality of fit was assessed statistically with an emphasis on ensuring that each of the parameters are physically sensible and are not highly correlated[2,3]. In the instance when the fit was poor, each $N_{Au-M}$ was introduced as a free parameter into the fits and the new best-fit values, subject to the EXAFS fit assessment criteria, were used as the constraints to refine the RMC simulation of the corresponding pair distribution function (PDF). EXAFS-enabled structure refinement was undertaken for BP7A PtPdAuCoCe, BP7A PtPdAuCoSn and Co2-P2 PtPdAuCoCe. The structure models, EXAFS fits and EXAFS fitting parameters for BP7A PtPdAuCoCe, BP7A PtPdAuCoSn and Co2-P2 PtPdAuCoCe before and after EXAFS-enabled structure refinement is shown in **Supplementary Fig. 9-10,** and **Supplementary Table 3**, respectively.

## Supplementary Note 2

Multitude of possible arrangement of atoms in HEA give rise to a continuous adsorption energy distribution pattern (AEDP), comprised of *n* number of adsorption peaks, where *n* is the number of elements in the HEA[4]. Herein, a simplified model using an electronic descriptor ($\psi$), which is known to be useful for predicting the adsorption energy of small molecules[5,6] has been used for understanding the AEDP in HEAs. Electronic descriptor ($\psi$) was calculated using the equation below, where $S_v$ is the number of valence electrons, $\chi$ is the electronegativity and $N$ is the number of atoms in the first nearest neighbouring shell. Note, the goal here is not to generalize the adsorption energies of HEAs but instead use the electronic descriptor as a proxy to underpin the differences in MOR activity of HEAs caused by adsorption energy shifts of constituent elements within AEDP. From a heterogeneous catalysis standpoint, adsorption occurs at the surfaces of catalyst surfaces. As such, we have undertaken the electronic descriptor calculations using surface atoms extracted from RMC generated structure models of HEAs. **Supplementary Fig. 14** shows the calculated AEDP of each constituent element in HEAs, visualized using kernel density plots. The slight negative tail in the distribution does not hold any physical meaning as it is merely an artifact of the gaussian kernel that has been applied over each data point. The broad distribution of $\psi$ is consistent with continuous AEDP reported previously[4,7,8]. The bi/trimodal features in the AEDP of each element is caused by the diverse local atomic neighbours it has at different sites, suggesting that each element in HEAs could have different electronic properties based on its neighbouring atoms[9], presenting an opportunity to modify the local adsorption properties of an active site by modulating the degree of alloying.

$$\psi = \frac{\left(\prod_{i=1}^{N} S_{v_i}\right)^{2/N}}{\left(\prod_{i=1}^{N} \chi_i\right)^{1/N}}$$

The inherent heterogeneity of HEAs would imply that small changes to the elemental composition and/or identity would have a dramatic effect on electronic properties, i.e., adsorption energy of active sites[10]. Any changes to the adsorption energy of the active sites would shift the individual adsorption peaks within AEDP, modulating the catalytic property depending on how much AEDP peak maxima has shifted from the optimal adsorption energy[7]. To extend our understanding about how individual

shifts in AEDP is influencing the catalytic properties, we are going to focus the discussion on just the adsorption energy of primary methanol electrooxidation active sites; platinum (Pt) and oxophillic (Ox) atoms, as shown in **Supplementary Fig. 15**. Synergistic interplay between Pt and Ox atoms is widely known to enhance the MOR activity, where Pt is the primary active site for methanol adsorption and dehydrogenation, and Ox promotes the oxidation of dehydrogenated methanol species by introducing $OH_{ads}$ upon the condition that Ox atoms are in proximity of Pt atoms[11,12]. The choice of assessing Pt and Ox is further rationalized by the fact that Au surfaces are generally inactive for MOR[13] and the composition of Pd on BP7A PtPdAuCoSn, BP7A PtPdAuCoSnCe and BP7A PtPdAuCoSnCeCu surfaces is less than 1 at. % (**Supplementary Table 4**), which we presume is not sufficient to be considered as a key active site in comparison to Pt atoms. For reference, we are using a pseudo-volcano plot under the assumption that peak maxima in BP7A PtPdAuCoSn's AEDP (2$^{nd}$ row; left) is located at the optimal adsorption energy, enabling us to make relative comparisons about how shifts in individual adsorption peaks are influencing the catalytic property. Assuming that Pt and Ox adsorption energy peak maxima in BP7A PtPdAuCoSn are positioned close to optimal binding energy is reasonable since it possess the lowest onset potential and highest anodic current response, both of which are strongly correlated to the position of adsorption energy in AEDP with respect to the optimal binding energy[8]. In the case of BP7A PtPdAuCoSn, we notice a maximum anodic current response ($j_A$) of 10.36 mA cm$^{-2}$ with an onset potential ($E_0$) of 450 mV, which can be attributed to peak maximum of Pt active site and Ox active sites located at/near the optimal binding energy. However, despite having a similar AEDP profile, BP7A PtPdAuCoCu, Co2-P2 PtPdAuCoCu and Co2-P2 PtPdAuCoSn has a lower anodic current response and higher onset potential, which might be due to unfavourable Pt-Pt and/or Pt-Ox coordination environment that is known to impact the methanol chemisorption behaviour and/or kinetics of methanol electrooxidation reaction[14,15]. In the case of BP7A PtPdAuCoSnCe, BP7A PtPdAuCoSnCeCu and Co2-P2 PtPdAuCoSnCe, we notice a considerably smaller and broader AEDP for both Pt and Ox, suggesting that there might not be enough active sites to elicit a similar anodic current response as BP7A PtPdAuCoSn[8]. Lastly, BP7A PtPdAuCoCe and Co2-P2 PtPdAuCoCe, where Ox atoms are significantly shifted towards left from the optimal binding energy, we notice a relatively higher onset potential and lower current response. We speculate the reason for higher onset potential is

likely due to the unfavourable adsorption energy for Ox, which would kinetically restrict the formation of key intermediate ($OH_{ads}$) in the early stages of methanol electrooxidation[16]. Furthermore, unfavourable binding energetics of Ox atom would prevent methanol adsorption and dehydrogenation on Pt sites by competing with those sites to produce $OH_{ads}$ that is required for methanol oxidation at higher potentials, resulting in lower maximum anodic current response. Overall, by using AEDP profile extracted from electronic descriptor built using our RMC structure models, our analysis has enabled us to form an understanding about how the shifts in individual adsorption energies within AEDP is influencing the catalytic properties of HEAs. We do acknowledge that the electronic descriptor model used here was built on assumptions about idealized local surface chemistry and structure, but for the purpose of understanding the origin of catalytic property differences in HEAs, we believe it has served the purpose. In the future, joint experimental and theoretical efforts that incorporates realistic HEA structure configurations will better enable us to form a more accurate understanding about the underlying working principle in HEAs.

# Supplementary Figures

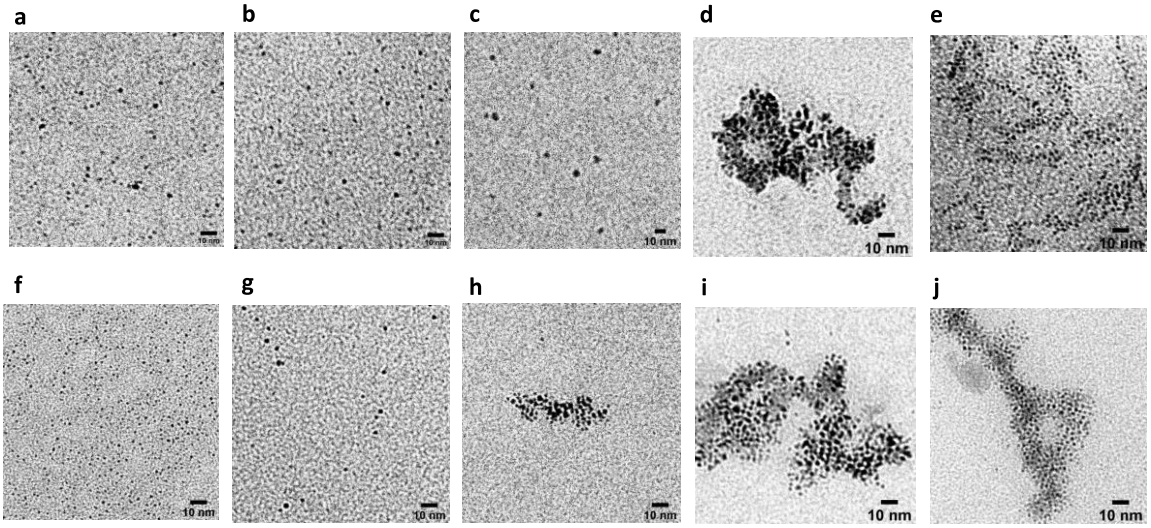


**Supplementary Fig. 1. TEM images of a) BP7A PtPdAuCoCu, b) BP7A PtPdAuCoSn, c) BP7A PtPdAuCoCe, d) BP7A PtPdAuCoSnCe, e) BP7A PtPdAuCoSnCeCu, f) Co2-P2 PtPdAuCoCu, g) Co2-P2 PtPdAuCoSn, h) Co2-P2 PtPdAuCoCe, i) Co2-P2 PtPdAuCoSnCe, and j) Co2-P2 PtPdAuCoSnCeCu.**

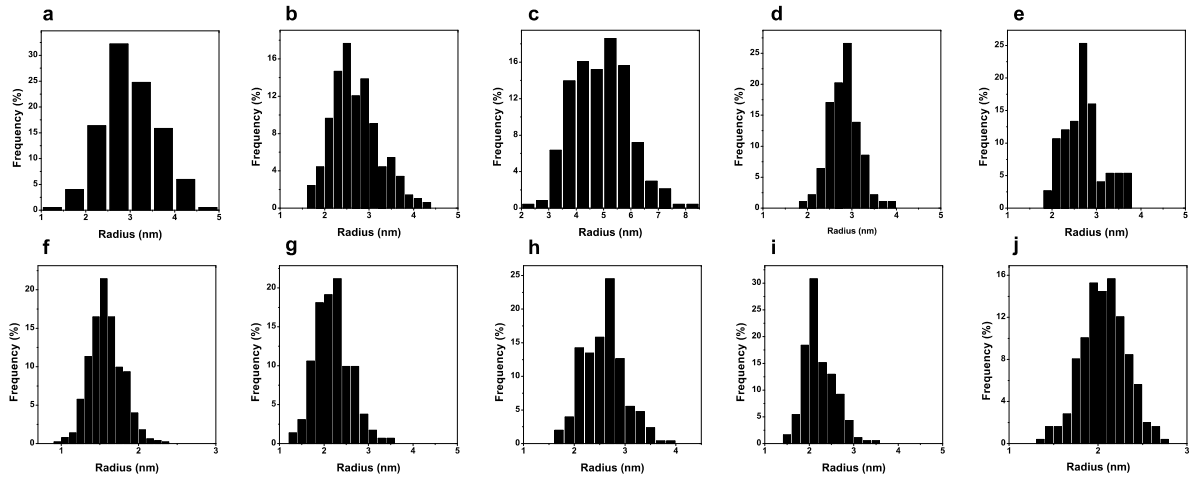


**Supplementary Fig. 2. Particle size distribution of a) BP7A PtPdAuCoCu, b) BP7A PtPdAuCoSn, c) BP7A PtPdAuCoCe, d) BP7A PtPdAuCoSnCe, e) BP7A PtPdAuCoSnCeCu, f) Co2-P2 PtPdAuCoCu, g) Co2-P2 PtPdAuCoSn, H) Co2-P2 PtPdAuCoCe, i) Co2-P2 PtPdAuCoSnCe, and j) Co2-P2 PtPdAuCoSnCeCu.**

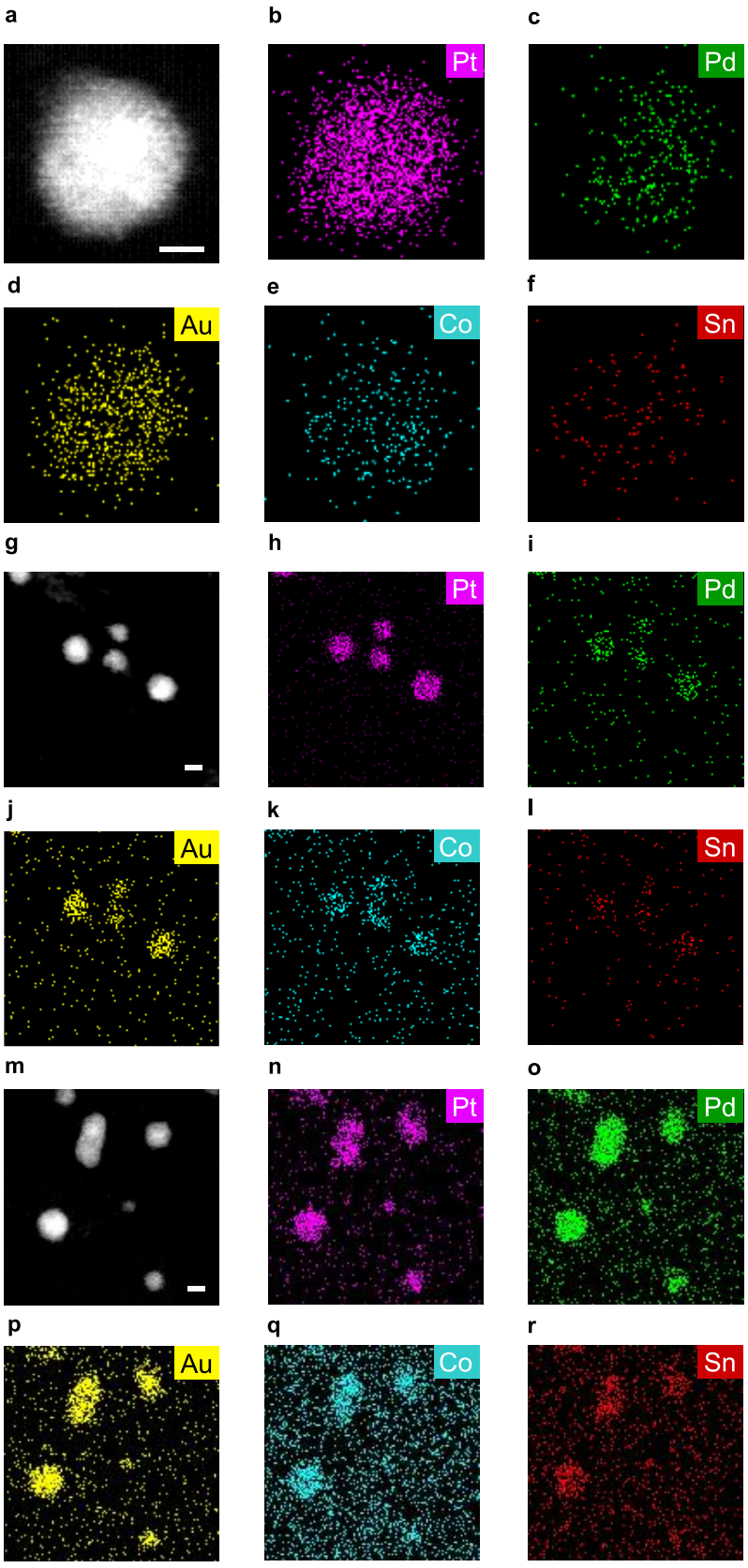


**Supplementary Fig. 3. EDS map of BP7A PtPdAuCoSn HEAs. Scale bar (a): 1 nm, and (g) & (m): 2 nm**

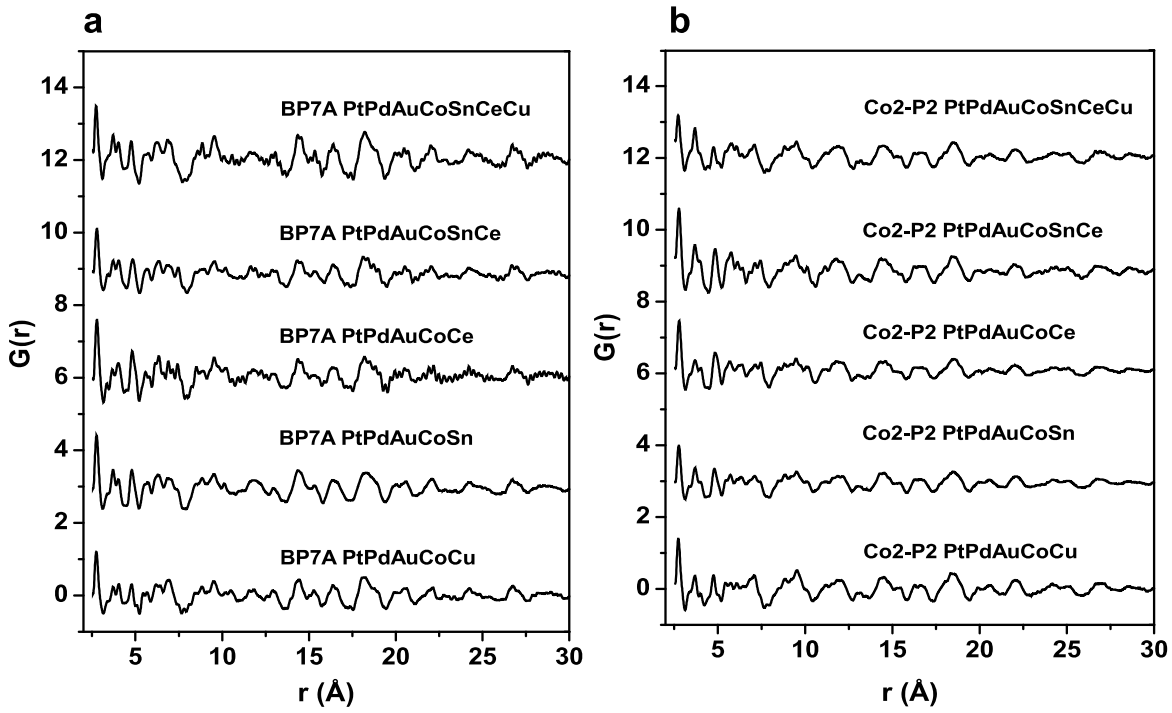


**Supplementary Fig. 4. Atomic PDFs of (a) BP7A HEAs and (b) Co2-P2 HEAs.**

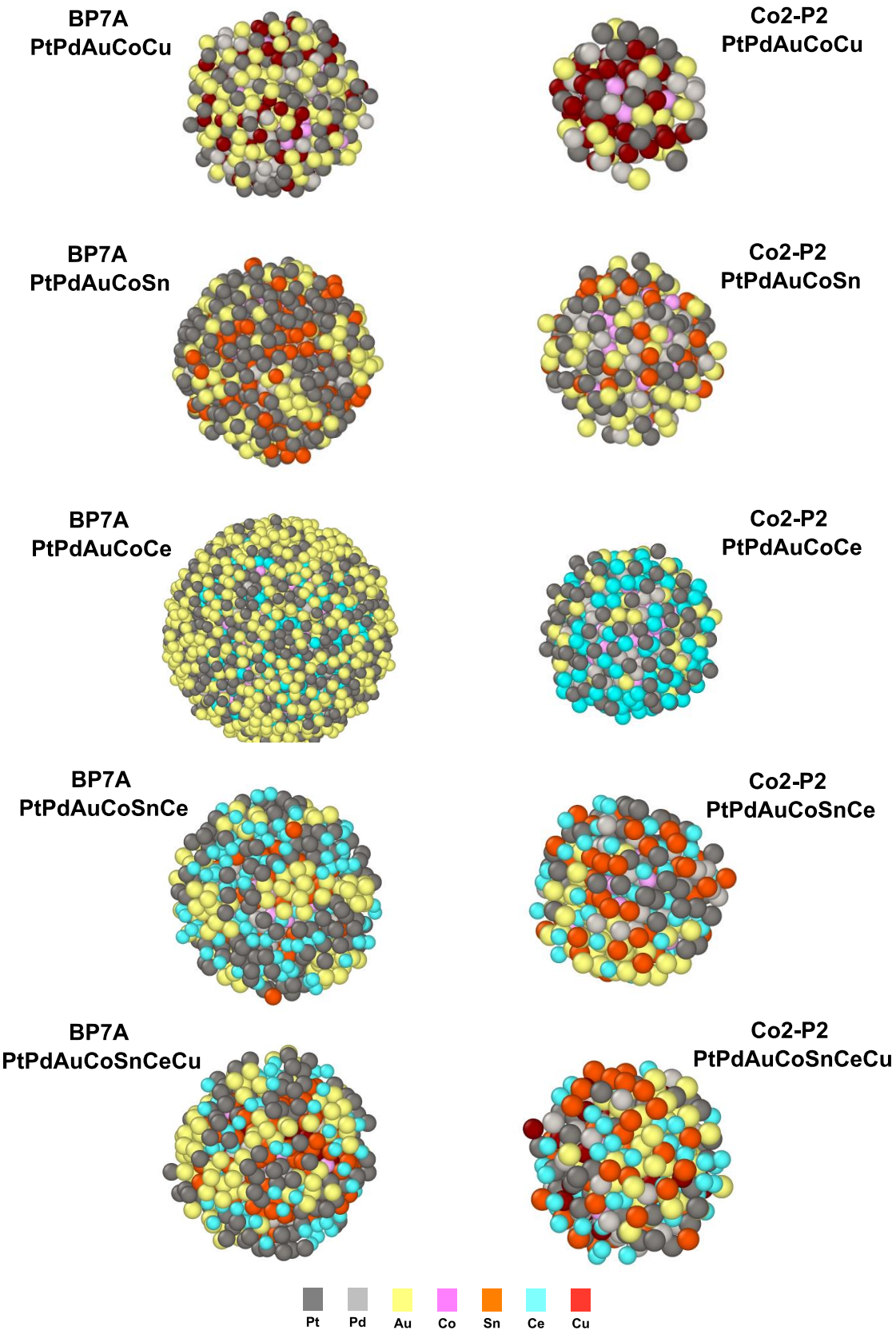


**Supplementary Fig. 5. Structure configuration of BP7A and Co2-P2 HEAs.**

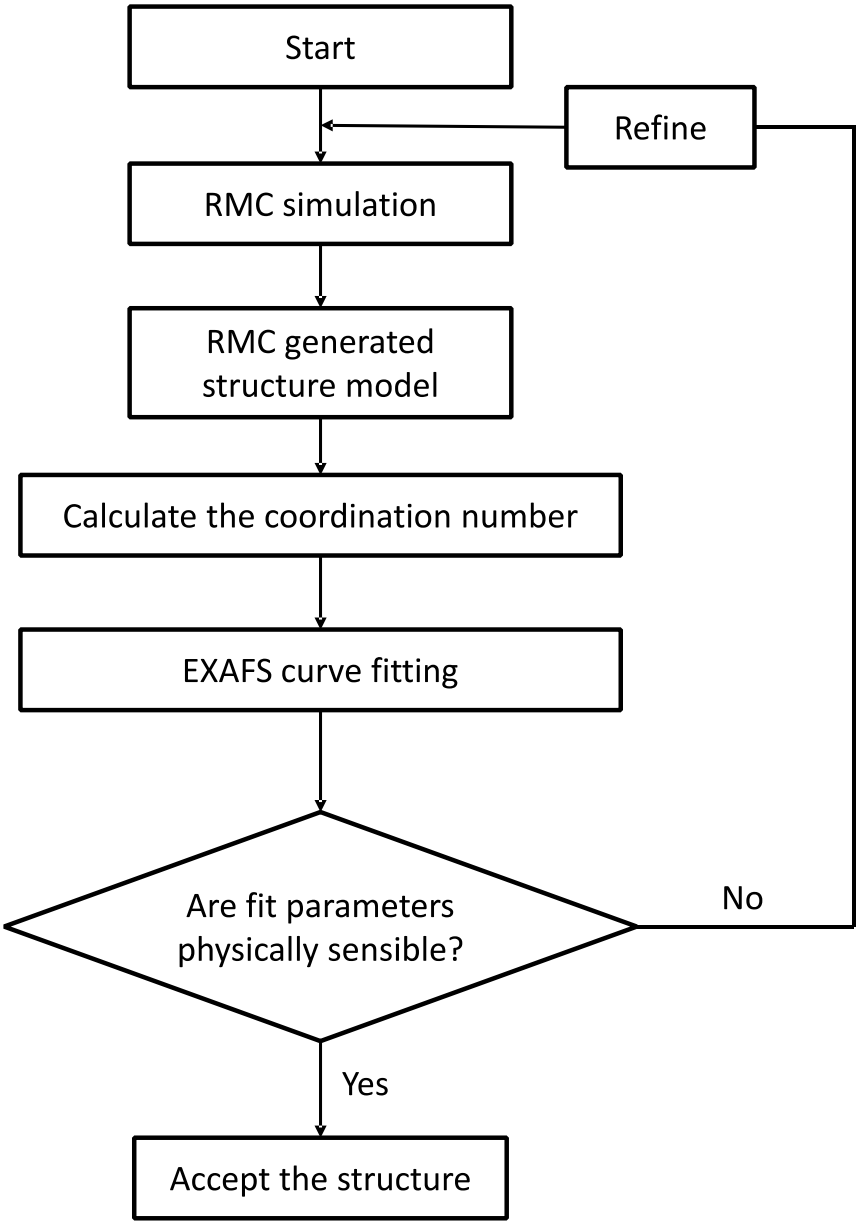


**Supplementary Fig. 6. Flowchart of RMC structure simulation workflow. See Supplementary Note 1 about structure refinement.**

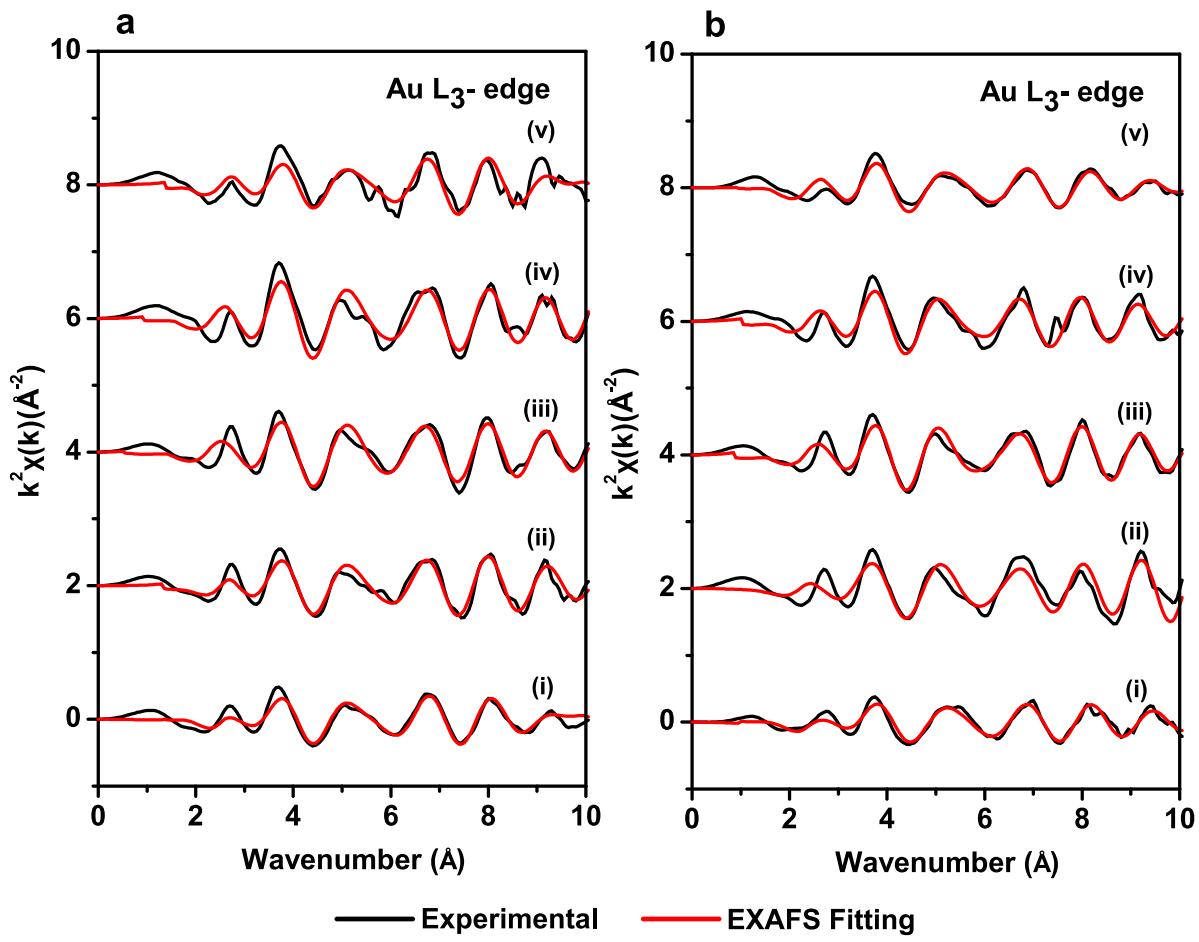


**Supplementary Fig. 7. EXAFS fitting of HEAs Au $L_3$ – edge in k-space for (a) BP7A, and (b) Co2-P2. Sample legend – (i) PtPdAuCoCu, (ii) PtPdAuCoSn, (iii) PtPdAuCoCe, (iv) PtPdAuCoSnCe, and (v) PtPdAuCoSnCeCu.**

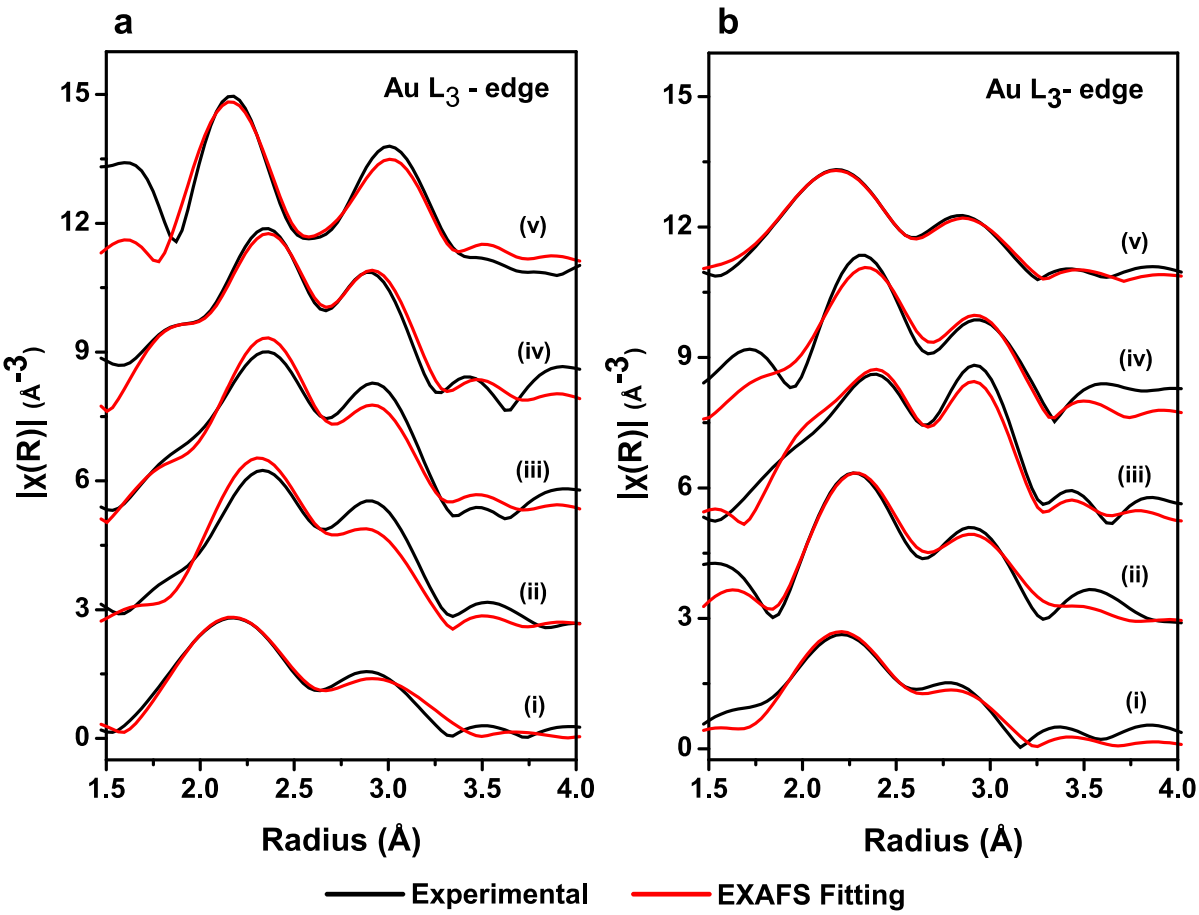


**Supplementary Fig. 8. EXAFS fitting of HEAs Au $L_3$ – edge in R-space for (a) BP7A, and (b) Co2-P2. Sample legend – (i) PtPdAuCoCu, (ii) PtPdAuCoSn, (iii) PtPdAuCoCe, (iv) PtPdAuCoSnCe, and (v) PtPdAuCoSnCeCu.**

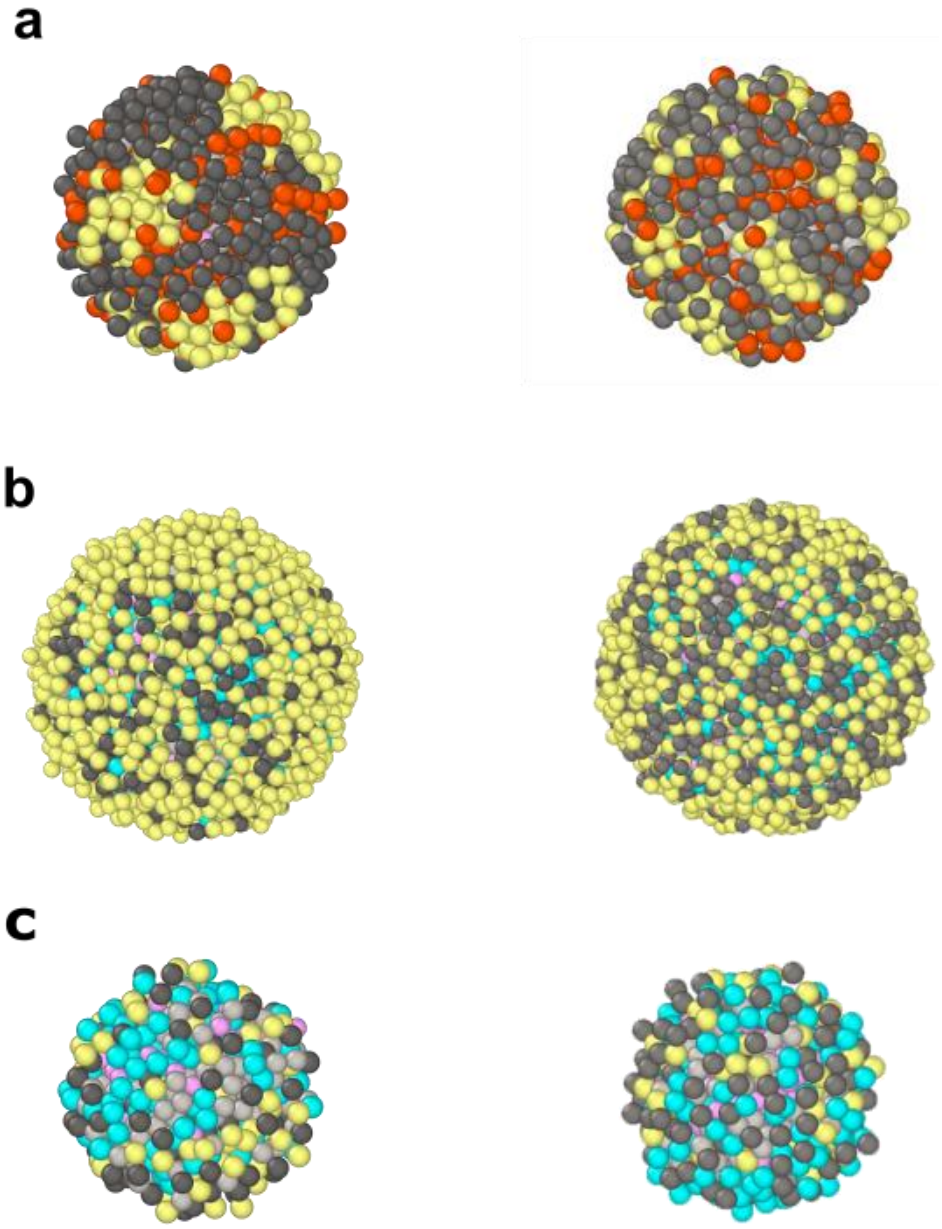


**Supplementary Fig. 9. Structure configuration before (left) and after (right) EXAFS-enabled structure refinement of (a) BP7A PtPdAuCoSn, (b) BP7A PtPdAuCoCe and (c) Co2-P2 PtPdAuCoCe**

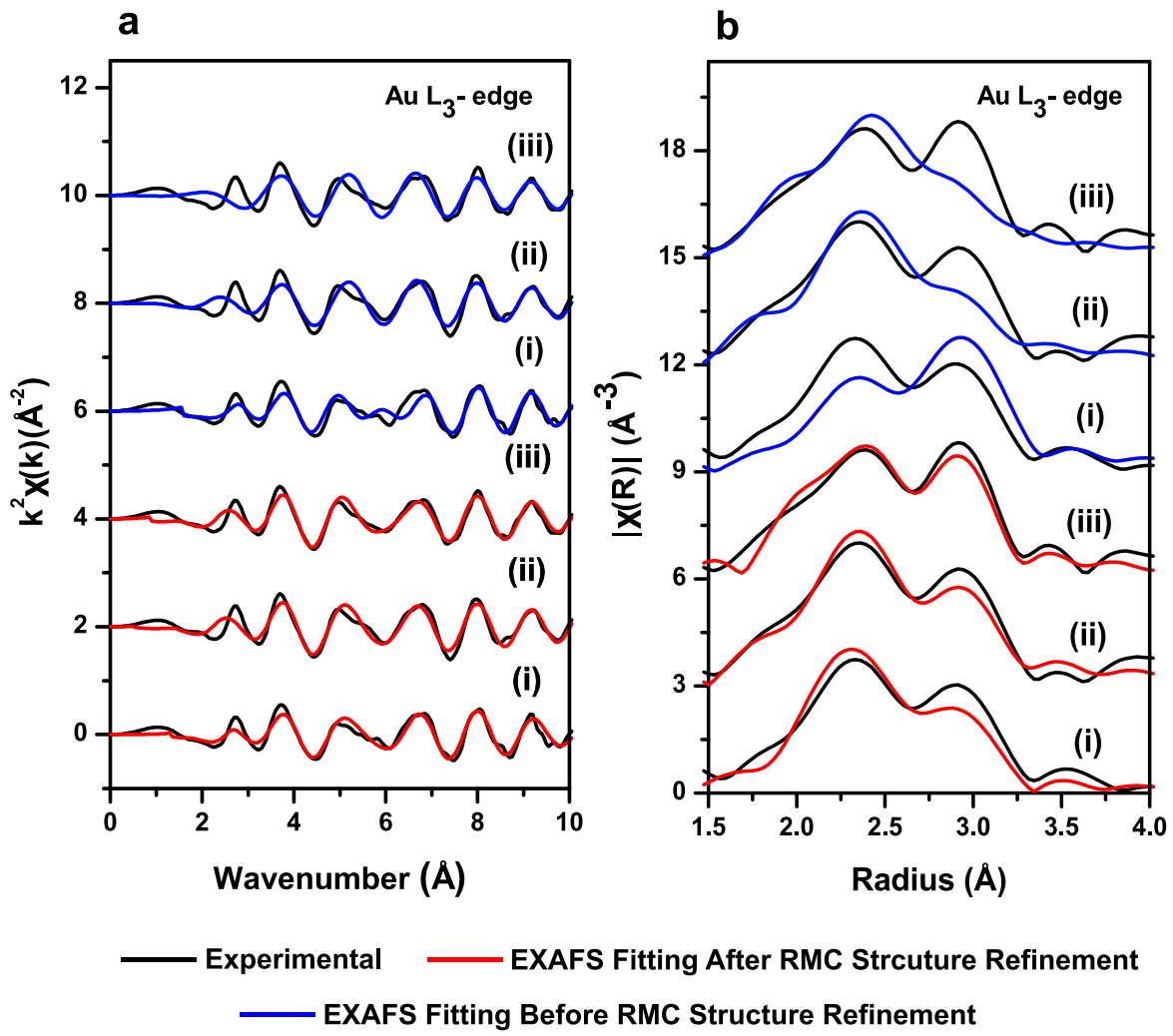


**Supplementary Fig. 10. EXAFS fitting of HEAs Au $L_3$ - edge of (a) k-space, and (b) R-space for (i) BP7A PtPdAuCoSn, (ii) BP7A PtPdAuCoCe, and (iii) Co2-P2 PtPdAuCoCe before and after RMC structure refinement**

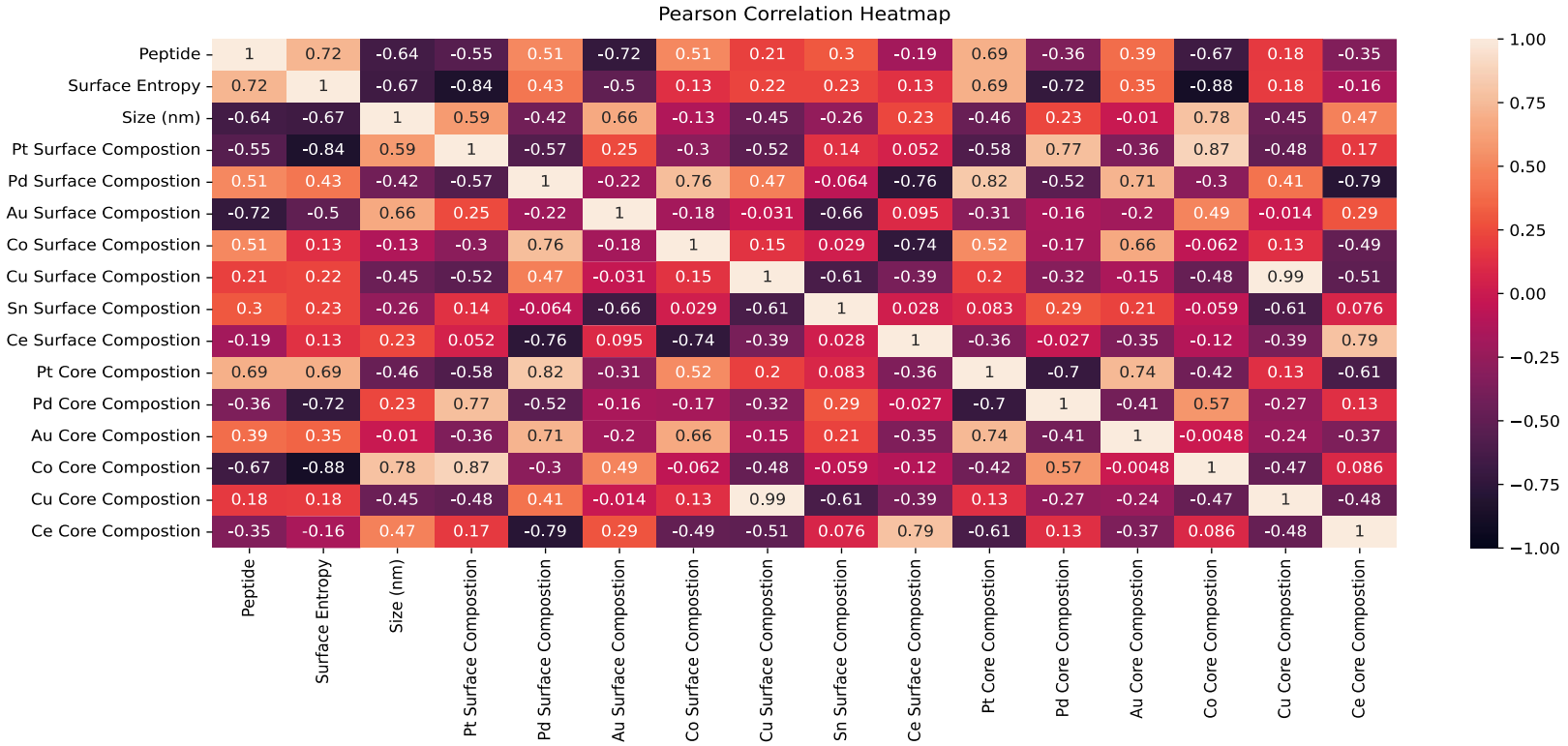


**Pearson correlation is calculated using method described in Supplementary Method*

**Supplementary Fig. 11. Correlation heatmap of surface and core elemental compositions from RMC model structures**

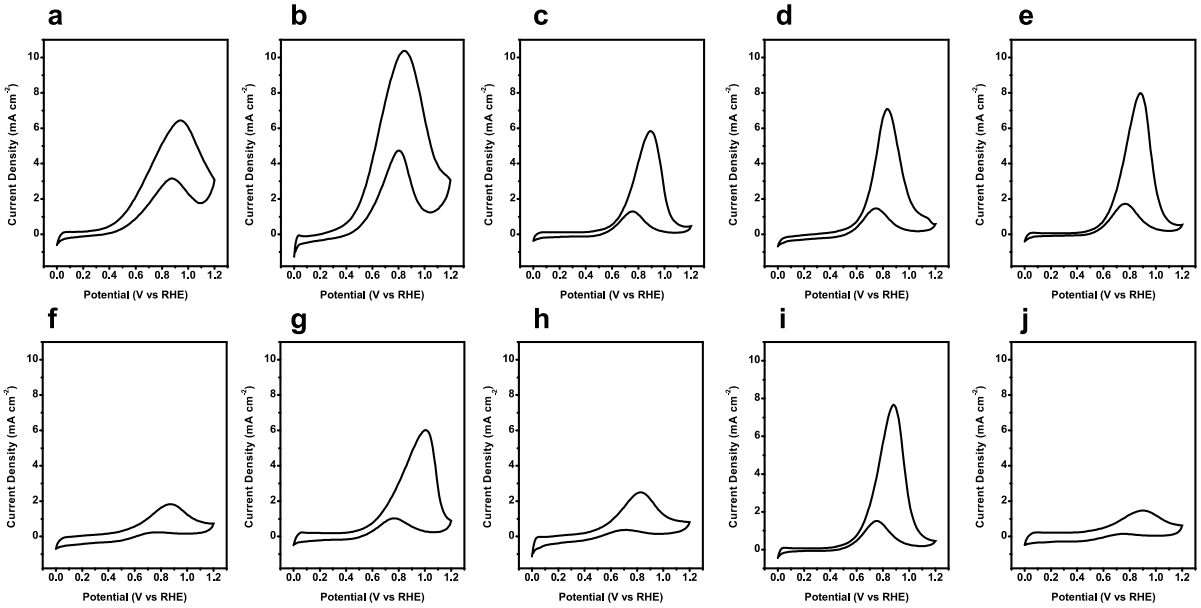


**Supplementary Fig. 12. Methanol oxidation cyclic voltammogram of a) BP7A PtPdAuCoCu, b) BP7A PtPdAuCoSn, c) BP7A PtPdAuCoCe, d) BP7A PtPdAuCoSnCe, e) BP7A PtPdAuCoSnCeCu, f) Co2-P2 PtPdAuCoCu, g) Co2-P2 PtPdAuCoSn, H) Co2-P2 PtPdAuCoCe, i) Co2-P2 PtPdAuCoSnCe, and j) Co2-P2 PtPdAuCoSnCeCu.**

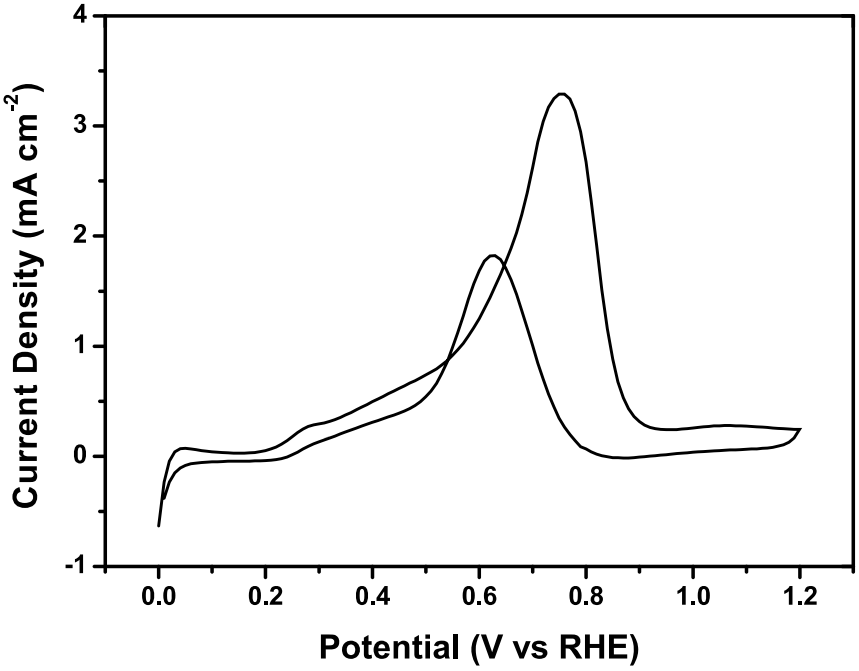


**Supplementary Fig. 13. Methanol oxidation cyclic voltammogram of Pt/C (20 wt.%)**

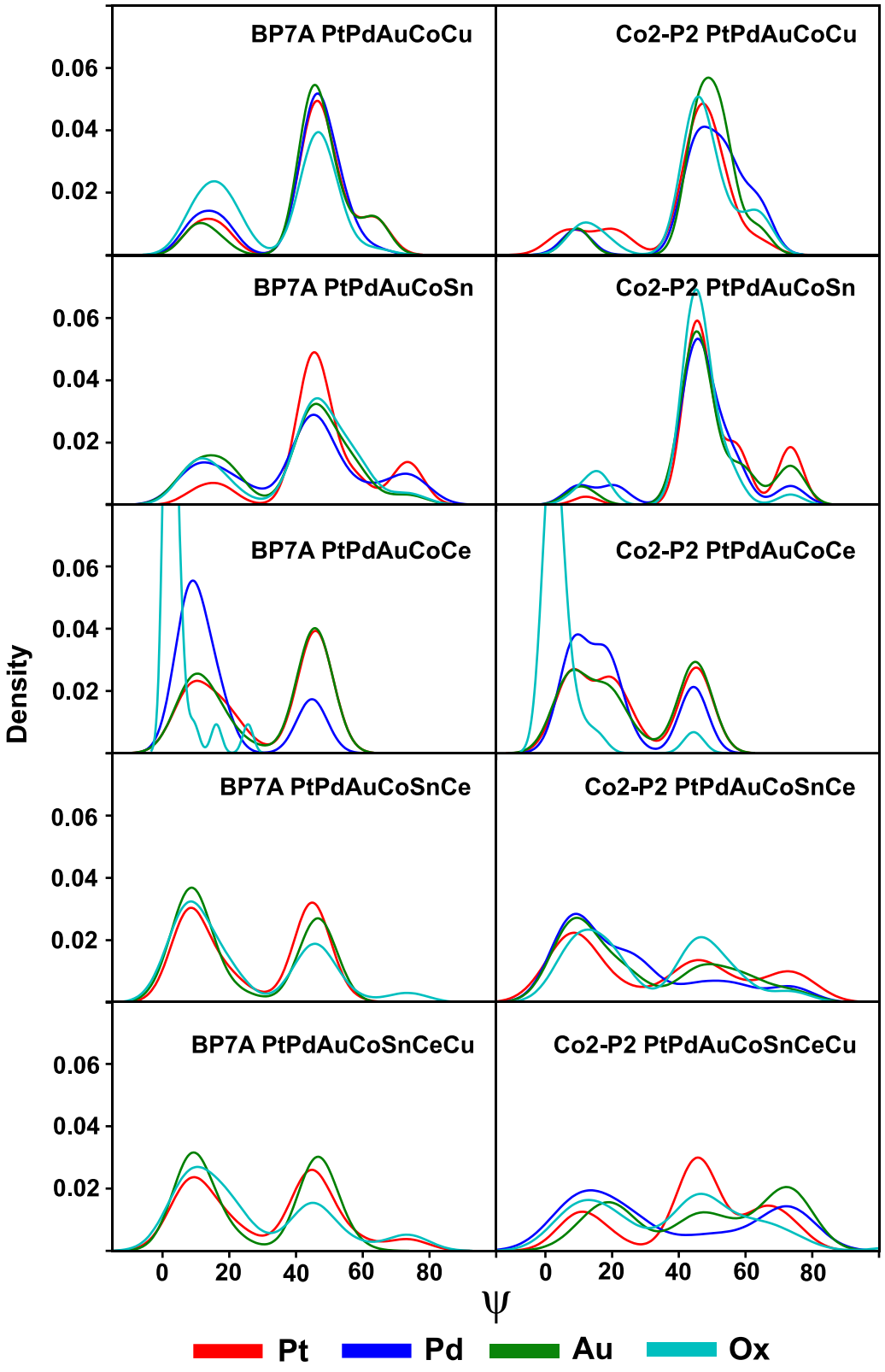


**Supplementary Fig. 14. Adsorption energy distribution pattern of constituent elements in HEAs; Platinum: Pt, Palladium: Pd Gold: Au, and Oxophillic atoms (Co, Sn, Ce and Cu): Ox**

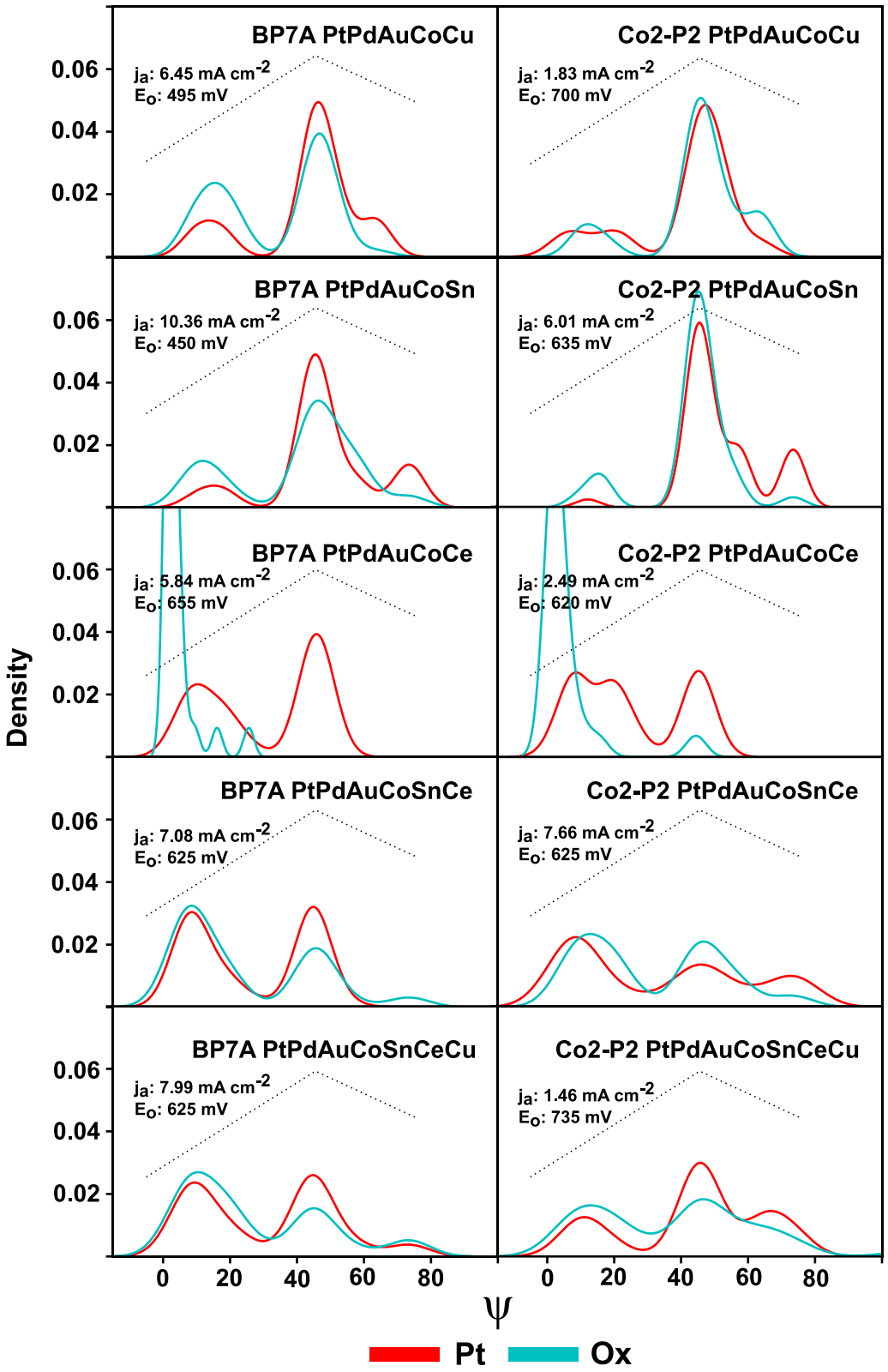


**Supplementary Fig. 15. Adsorption energy distribution pattern of primary active sites in HEAs; Platinum: Pt, and Oxophillic atoms (Co, Sn, Ce and Cu): Ox. Dashed line indicates the pseudo-volcano plot, placed under the assumption that AEDP of BP7A PtPdAuCoSn possess peak maxima at optimal adsorption**

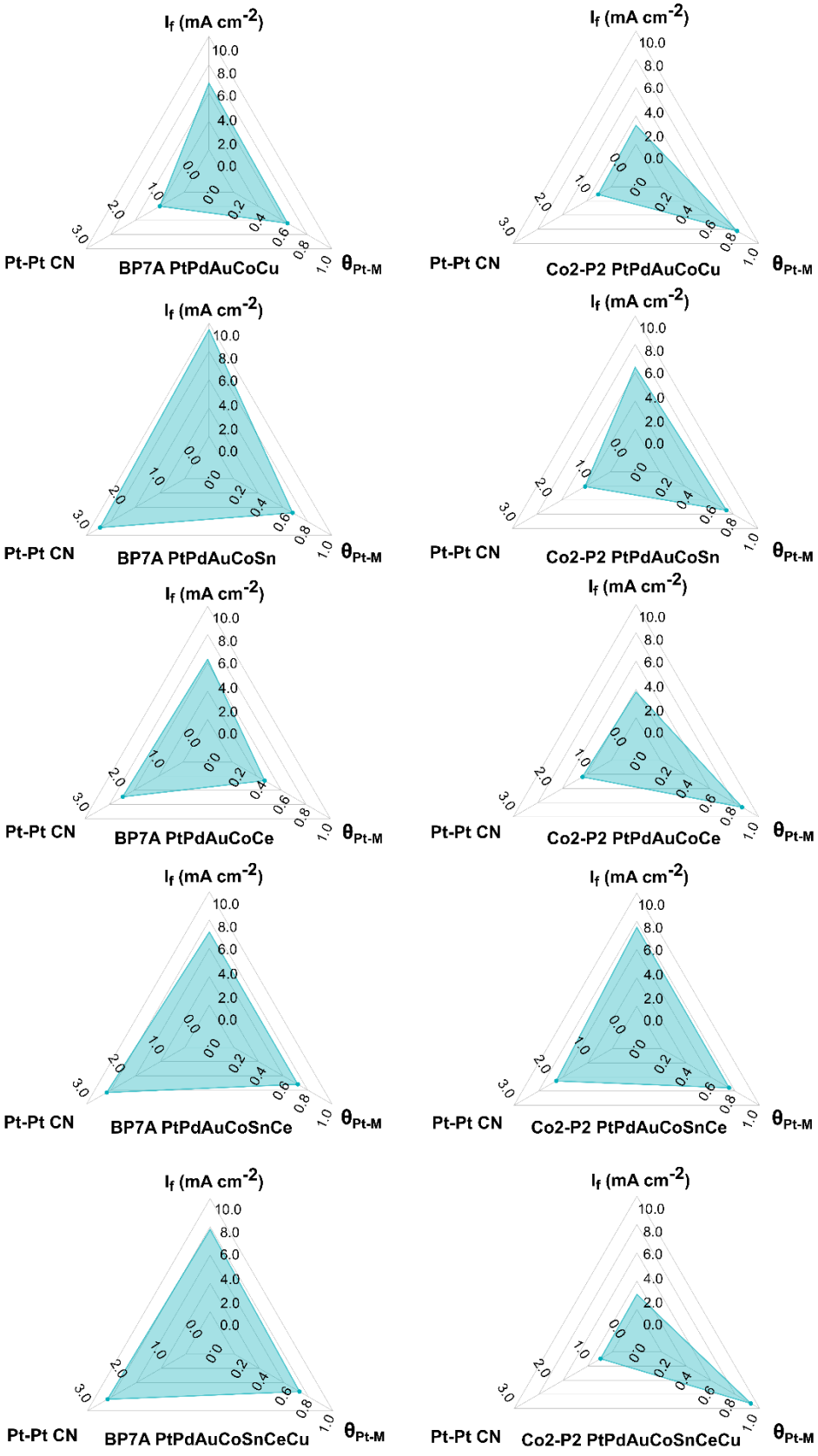


$I_f$: Forward peak current density,
$\theta_{Pt-M}$: Fraction of surface Pt atoms with atleast one oxophillic atom in the proximity,
Pt-Pt CN: Average surface Pt-Pt coordination number

**Supplementary Fig. 16. Radar plots of HEAs**

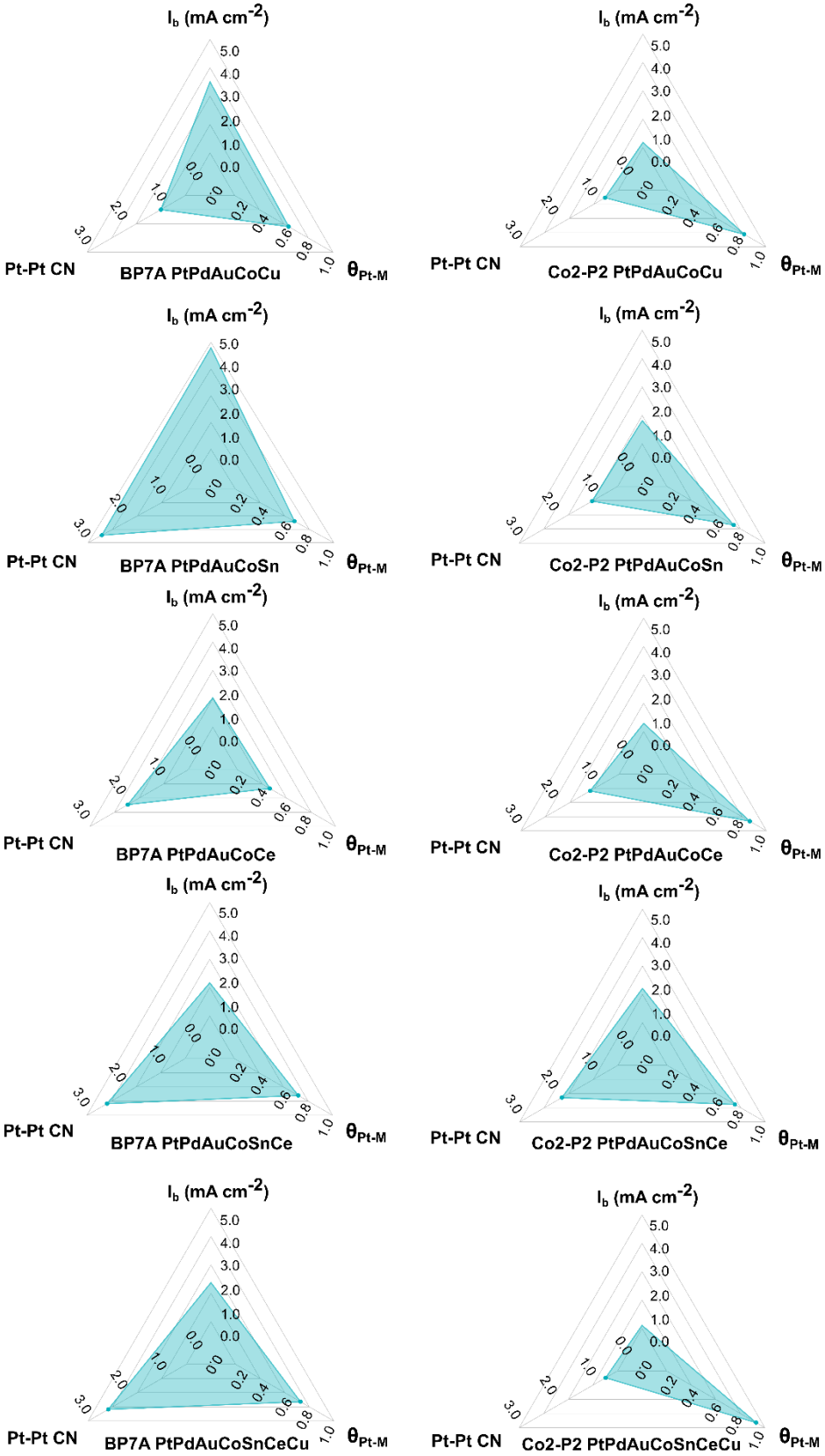


$I_b$ : Backward peak current density,
$\theta_{Pt-M}$: Fraction of surface Pt atoms with atleast one oxophillic atom in the proximity,
Pt-Pt CN: Average surface Pt-Pt coordination number

**Supplementary Fig. 17. Radar plots of HEAs**

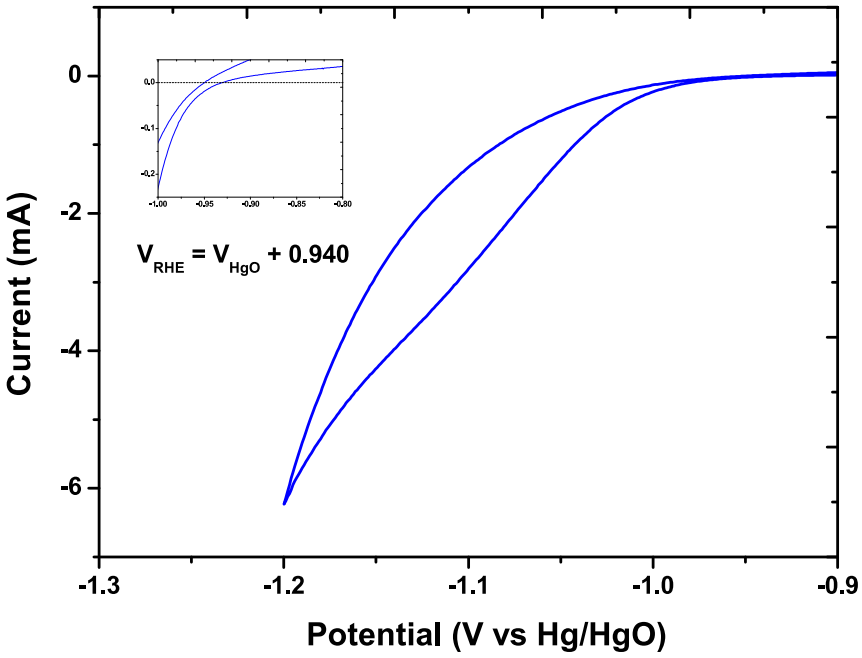


**Supplementary Fig. 18. Hg/HgO reference electrode calibration**

# Supplementary Tables

**Supplementary Table 1 – Inductively coupled mass-spectroscopy (ICP-MS) of HEAs**

| Sample | Elemental Composition (mol.%) | | | | | | | Configurational Entropy (kJ $mol^{-1} K^{-1}$) |
|---|---|---|---|---|---|---|---|---|
| | Pt | Pd | Au | Co | Cu | Sn | Ce | |
| BP7A PtPdAuCoCu | 24.76 ± 1.24 | 16.08 ± 0.80 | 28.92 ± 1.45 | 9.49 ± 0.47 | 20.52 ± 1.03 | | | 1.55R ± 0.04 |
| BP7A PtPdAuCoSn | 31.93 ± 1.60 | 15.71 ± 0.79 | 17.54 ± 0.88 | 11.95 ± 0.60 | | 22.87 ± 1.14 | | 1.55R ± 0.04 |
| BP7A PtPdAuCoCe | 21.68 ± 1.08 | 14.70 ± 0.74 | 23.59 ± 1.18 | 14.29 ± 0.71 | | | 25.74 ± 1.29 | 1.58R ± 0.04 |
| BP7A PtPdAuCoSnCe | 22.73 ± 1.14 | 10.96 ± 0.55 | 20.52 ± 1.03 | 5.68 ± 0.28 | | 16.41 ± 0.82 | 23.70 ± 1.19 | 1.70R ± 0.04 |
| BP7A PtPdAuCoSnCeCu | 21.73 ± 1.09 | 10.68 ± 0.53 | 16.30 ± 0.82 | 4.74 ± 0.24 | 8.67 ± 0.43 | 22.79 ± 1.14 | 15.09 ± 0.75 | 1.84R ± 0.04 |
| Co2-P2 PtPdAuCoCu | 22.96 ± 1.15 | 17.20 ± 0.86 | 17.30 ± 0.87 | 6.26 ± 0.31 | 36.29 ± 1.81 | | | 1.49R ± 0.04 |
| Co2-P2 PtPdAuCoSn | 29.87 ± 1.49 | 19.32 ± 0.97 | 23.72 ± 1.19 | 10.74 ± 0.54 | | 16.35 ± 0.82 | | 1.56R ± 0.04 |
| Co2-P2 PtPdAuCoCe | 22.07 ± 1.10 | 20.94 ± 1.05 | 20.70 ± 1.04 | 12.06 ± 0.60 | | | 24.23 ± 1.21 | 1.59R ± 0.04 |
| Co2-P2 PtPdAuCoSnCe | 24.23 ± 1.21 | 14.16 ± 0.71 | 17.25 ± 0.86 | 6.64 ± 0.33 | | 16.96 ± 0.85 | 20.76 ± 1.04 | 1.73R ± 0.04 |
| Co2-P2 PtPdAuCoSnCeCu | 21.75 ± 1.09 | 12.85 ± 0.64 | 17.02 ± 0.85 | 2.35 ± 0.12 | 8.66 ± 0.43 | 18.14 ± 0.91 | 19.23 ± 0.96 | 1.82R ± 0.04 |

**Configurational entropy is calculated using method described in Supplementary Method*

## Supplementary Table 2 – EXAFS Fitting Parameters

| Peptide | Sample | $S_0^2$ | ΔE (eV) | σ (Å²) | $\Delta R_{Au-Pt}$ (Å) | $\Delta R_{Au-Pd}$ (Å) | $\Delta R_{Au-Au}$ (Å) | $\Delta R_{Au-Co}$ (Å) | $\Delta R_{Au-Cu}$ (Å) | $\Delta R_{Au-Sn}$ (Å) | $\Delta R_{Au-Ce}$ (Å) | R-factor | $N_{Au-Pt}$ | $N_{Au-Pd}$ | $N_{Au-Au}$ | $N_{Au-Co}$ | $N_{Au-Cu}$ | $N_{Au-Sn}$ | $N_{Au-Ce}$ |
|---|---|---|---|---|---|---|---|---|---|---|---|---|---|---|---|---|---|---|---|
| BP7A | PtPdAuCoCu | 0.85 | 6.811 ± 5.911 | 0.005 ± 0.003 | 0.064 ± 0.079 | 0.088 ± 0.087 | 0.093 ± 0.056 | 0.087 ± 0.075 | -0.130 ± 0.043 | | | 0.030 | 1.6 | 1.4 | 1.5 | 1.7 | 2.1 | | |
| | PtPdAuCoSn | 0.85 | 6.762 ± 7.241 | 0.008 ± 0.004 | 0.051 ± 0.091 | -0.004 ± 0.030 | 0.062 ± 0.103 | -0.024 ± 0.069 | | 0.099 ± 0.083 | | 0.032 | 1.5 | 2.0 | 1.8 | 2.0 | | 1.8 | |
| | PtPdAuCoCe | 0.85 | 1.145 ± 4.215 | 0.004 ± 0.004 | -0.021 ± 0.062 | -0.013 ± 0.077 | -0.006 ± 0.056 | 0.002 ± 0.077 | | | 0.070 ± 0.075 | 0.034 | 1.7 | 2.9 | 1.8 | 1.9 | | | 2.2 |
| | PtPdAuCoSnCe | 0.85 | 3.477 ± 4.082 | 0.003 ± 0.002 | -0.015 ± 0.022 | -0.064 ± 0.053 | -0.000 ± 0.097 | -0.010 ± 0.060 | | 0.007 ± 0.071 | 0.107 ± 0.064 | 0.054 | 1.3 | 1.7 | 2.9 | 1.0 | | 1.8 | 1.5 |
| | PtPdAuCoSnCeCu | 0.85 | 7.072 ± 3.207 | 0.004 ± 0.002 | 0.051 ± 0.078 | 0.011 ± 0.078 | 0.101 ± 0.053 | -0.093 ± 0.041 | 0.064 ± 0.069 | 0.040 ± 0.033 | 0.116 ± 0.036 | 0.044 | 1.1 | 1.3 | 1.6 | 1.0 | 1.0 | 1.4 | 1.2 |
| Co2-P2 | PtPdAuCoCu | 0.85 | 3.458 ± 6.505 | 0.010 ± 0.003 | 0.026 ± 0.050 | 0.022 ± 0.059 | -0.025 ± 0.040 | 0.051 ± 0.093 | -0.122 ± 0.054 | | | 0.040 | 1.5 | 1.5 | 1.5 | 1.7 | 2.1 | | |
| | PtPdAuCoSn | 0.85 | 0.000 ± 5.935 | 0.003 ± 0.001 | -0.053 ± 0.093 | -0.096 ± 0.018 | -0.051 ± 0.094 | -0.039 ± 0.083 | | 0.058 ± 0.029 | | 0.035 | 1.5 | 2.0 | 1.5 | 1.6 | | 1.5 | |
| | PtPdAuCoCe | 0.85 | 2.781 ± 1.724 | 0.002 ± 0.001 | -0.058 ± 0.022 | 0.008 ± 0.042 | 0.058 ± 0.035 | 0.027 ± 0.040 | | | 0.070 ± 0.060 | 0.036 | 1.7 | 2.8 | 2.1 | 1.7 | | | 1.7 |
| | PtPdAuCoSnCe | 0.85 | 4.067 ± 5.251 | 0.009 ± 0.007 | 0.016 ± 0.067 | 0.056 ± 0.083 | 0.054 ± 0.049 | -0.001 ± 0.107 | | -0.095 ± 0.095 | 0.073 ± 0.107 | 0.046 | 1.8 | 2.1 | 2.6 | 1.4 | | 1.4 | 1.6 |
| | PtPdAuCoSnCeCu | 0.85 | 3.161 ± 3.595 | 0.009 ± 0.004 | -0.052 ± 0.084 | 0.059 ± 0.079 | -0.019 ± 0.085 | -0.118 ± 0.048 | 0.041 ± 0.088 | -0.091 ± 0.076 | 0.063 ± 0.084 | 0.016 | 1.7 | 1.4 | 1.5 | 1.1 | 1.6 | 1.4 | 1.3 |

**Supplementary Table 3 – EXAFS Fitting Parameters Before and After EXAFS-enabled RMC Structure Refinement**

| | Peptide | Sample | $S_0^2$ | ΔE (eV) | σ (Å²) | $\Delta R_{Au-Pt}$ (Å) | $\Delta R_{Au-Pd}$ (Å) | $\Delta R_{Au-Au}$ (Å) | $\Delta R_{Au-Co}$ (Å) | $\Delta R_{Au-Cu}$ (Å) | $\Delta R_{Au-Sn}$ (Å) | $\Delta R_{Au-Ce}$ (Å) | R-factor | $N_{Au-Pt}$ | $N_{Au-Pd}$ | $N_{Au-Au}$ | $N_{Au-Co}$ | $N_{Au-Cu}$ | $N_{Au-Sn}$ | $N_{Au-Ce}$ |
|---|---|---|---|---|---|---|---|---|---|---|---|---|---|---|---|---|---|---|---|---|
| Before | BP7A | PtPdAuCoSn | 0.85 | 9.299 ± 8.043 | 0.003 ± 0.025 | 0.088 ± 1.367 | 0.019 ± 0.129 | 0.062 ± 1.121 | - | | 0.122 ± 0.207 | | 0.134 | 1.5 | 1.6 | 1.7 | - | | 1.7 | |
| | | PtPdAuCoCe | 0.85 | -2.400 ± 9.567 | 0.001 ± 0.002 | -0.104 ± 0.175 | -0.047 ± 0.128 | -0.035 ± 0.104 | -0.038 ± 0.125 | | | 0.069 ± 0.110 | 0.098 | 1.5 | 1.2 | 1.4 | 1.4 | | | 1.6 |
| | Co2P2 | PtPdAuCoCe | 0.85 | - 17.77 ± 6.978 | 0.006 ± 0.003 | -0.486 ± 0.054 | -0.268 ± 0.082 | 0.250 ± 0.067 | -0.255 ± 0.086 | | | 0.000 ± 0.062 | 0.180 | 1.9 | 1.8 | 2.2 | 1.8 | | | 1.9 |
| After | BP7A | PtPdAuCoSn | 0.85 | 6.762 ± 7.241 | 0.008 ± 0.004 | 0.051 ± 0.091 | -0.004 ± 0.030 | 0.062 ± 0.103 | -0.024 ± 0.069 | | 0.099 ± 0.083 | | 0.032 | 1.5 | 2.0 | 1.8 | 2.0 | | 1.8 | |
| | | PtPdAuCoCe | 0.85 | 1.145 ± 4.215 | 0.004 ± 0.004 | -0.021 ± 0.062 | -0.013 ± 0.077 | -0.006 ± 0.056 | 0.002 ± 0.077 | | | 0.070 ± 0.075 | 0.034 | 1.7 | 2.9 | 1.8 | 1.9 | | | 2.2 |
| | Co2P2 | PtPdAuCoCe | 0.85 | 2.781 ± 1.724 | 0.002 ± 0.001 | -0.058 ± 0.022 | 0.008 ± 0.042 | 0.058 ± 0.035 | 0.027 ± 0.040 | | | 0.070 ± 0.060 | 0.036 | 1.7 | 2.8 | 2.1 | 1.7 | | | 1.7 |

**Supplementary Table 4 – Surface composition of Pt and Pd**

| Sample | Pt composition (at %) | Pd composition (at %) |
|---|---|---|
| BP7A PtPdAuCoCu | 33.45 | 18.5 |
| BP7A PtPdAuCoSn | 63.13 | 3.45 |
| BP7A PtPdAuCoCe | 50 | 1.00 |
| BP7A PtPdAuCoSnCe | 38.44 | 0.00 |
| BP7A PtPdAuCoSnCeCu | 42.31 | 0.00 |
| Co2P2 PtPdAuCoCu | 31.08 | 22.97 |
| Co2P2 PtPdAuCoSn | 36.36 | 11.93 |
| Co2P2 PtPdAuCoCe | 36.04 | 11.24 |
| Co2P2 PtPdAuCoSnCe | 28.07 | 6.43 |
| Co2P2 PtPdAuCoSnCeCu | 20.36 | 13.17 |

**Supplementary Table 5 – $I_f/I_b$ of MOR CVs**

| Sample | $I_f/I_b$ |
|---|---|
| BP7A PtPdAuCoCu | 2.1 |
| BP7A PtPdAuCoSn | 2.2 |
| BP7A PtPdAuCoCe | 5.7 |
| BP7A PtPdAuCoSnCe | 4.8 |
| BP7A PtPdAuCoSnCeCu | 4.6 |
| Co2-P2 PtPdAuCoCu | 8.3 |
| Co2-P2 PtPdAuCoSn | 5.9 |
| Co2-P2 PtPdAuCoCe | 6.2 |
| Co2-P2 PtPdAuCoSnCe | 5.1 |
| Co2-P2 PtPdAuCoSnCeCu | 11.2 |

## Supplementary References


1 Yeh, J.-W. in *High-Entropy Alloys: Fundamentals and Applications* (eds Michael C. Gao, Jien-Wei Yeh, Peter K. Liaw, & Yong Zhang) 1-19 (Springer International Publishing, 2016).

2 Calvin, S. *XAFS for Everyone*. (CRC press, 2013).

3 Kelly, S., Hesterberg, D. & Ravel, B. Analysis of soils and minerals using X-ray absorption spectroscopy. *Methods of soil analysis part 5—mineralogical methods* **5**, 387-463.

4 Batchelor, T. A. A. *et al.* High-Entropy Alloys as a Discovery Platform for Electrocatalysis. *Joule* **3**, 834-845.

5 Gao, W. *et al.* Determining the adsorption energies of small molecules with the intrinsic properties of adsorbates and substrates. *Nature Communications* **11**, 1196.

6 Roy, D., Mandal, S. C. & Pathak, B. Machine Learning Assisted Exploration of High Entropy Alloy-Based Catalysts for Selective CO2 Reduction to Methanol. *The Journal of Physical Chemistry Letters* **13**, 5991-6002.

7 Löffler, T. *et al.* Design of Complex Solid-Solution Electrocatalysts by Correlating Configuration, Adsorption Energy Distribution Patterns, and Activity Curves. *Angewandte Chemie International Edition* **59**, 5844-5850.

8 Löffler, T. *et al.* Comparing the Activity of Complex Solid Solution Electrocatalysts Using Inflection Points of Voltammetric Activity Curves as Activity Descriptors. *ACS Catalysis* **11**, 1014-1023.

9 Wu, D. *et al.* Noble-Metal High-Entropy-Alloy Nanoparticles: Atomic-Level Insight into the Electronic Structure. *Journal of the American Chemical Society* **144**, 3365-3369.

10 Choksi, T. S., Roling, L. T., Streibel, V. & Abild-Pedersen, F. Predicting Adsorption Properties of Catalytic Descriptors on Bimetallic Nanoalloys with Site-Specific Precision. *The Journal of Physical Chemistry Letters* **10**, 1852-1859.

11 Iwasita, T. Electrocatalysis of methanol oxidation. *Electrochimica Acta* **47**, 3663-3674.

12 Zhuang, L., Jin, J. & Abruña, H. D. Direct Observation of Electrocatalytic Synergy. *Journal of the American Chemical Society* **129**, 11033-11035.

13 Xiao, S. *et al.* Hierarchical Nanoporous Gold-Platinum with Heterogeneous Interfaces for Methanol Electrooxidation. *Scientific Reports* **4**, 4370.

14 Wei, A., Feng, W., Liu, H., Huang, X. & Yang, G. Methanol activation catalyzed by Pt7, Pt3Cu4, and Cu7 clusters: A density functional theory investigation. *Applied Organometallic Chemistry* **32**, e4197.

15 You, G. *et al.* PtPd(111) Surface versus PtAu(111) Surface: Which One Is More Active for Methanol Oxidation? *ACS Catalysis* **8**, 132-143.

16 Chung, D. Y., Lee, K.-J. & Sung, Y.-E. Methanol Electro-Oxidation on the Pt Surface: Revisiting the Cyclic Voltammetry Interpretation. *The Journal of Physical Chemistry C* **120**, 9028-9035.